Isolation Methods Influence the Protein Corona Composition on Gold-coated Iron Oxide Nanoparticles

Khoi Nguyen L. Hoang, †Korin E. Wheeler, ‡ and Catherine J. Murphy*,†

ABSTRACT: Upon exposure to a biological environment, nanoparticles (NPs) acquire biomolecular coatings, the most studied of which is the protein corona. This protein corona gives NPs a new biological identity that will determine various biological responses including cellular uptake, biodistribution, and toxicity. The standard method to isolate NPs from a biological matrix in order to study their coronas is centrifugation, but more gentle means of retrieval may enable deeper understanding of both irreversibly bound hard coronas and more loosely bound soft coronas. In this study, magnetic gold-coated iron oxide NPs were incubated with rainbow trout gill cell total protein extracts and mass spectrometric proteomic analysis was conducted to determine the composition of the protein coronas isolated by either centrifugation or magnetic retrieval. The number of washes were varied to strip away the soft coronas and isolate the hard corona. Hundreds of proteins were adsorbed to the NPs. Some proteins were common to all isolation methods, and many others were particular to the isolation method. Some qualitative trends in protein character where discerned from quantitative proteomic analyses, but more importantly, a new kind of protein corona was identified: mixed corona, in which the labile or inert nature of the protein-NP interaction is dependent upon sample history.

The use of engineered nanoparticles (NPs) in numerous applications has been growing rapidly in the past few decades. This growth is driven by the unique chemical and physical properties that stems from their nanoscale size. These NP are being applied to better the human experience; for example, NPs are being used for applications in health and medicine (e.g., diagnostic chemical sensing, cellular imaging, drug delivery, therapeutics).^{2–7} However, negative NP effects at the cellular and organism levels in some cases give the community pause before wide-scale implementation.^{8–11} A mechanistic understanding of the impact of NPs informs risk assessments and enables development of more sustainable nanotechnologies.^{1,12–16}

The biochemistry of NPs complicates predictions of their biological impacts. Upon exposure to biological environment, biomolecules such as proteins, lipids, sugars or even DNA, adsorb onto the NP surface. 16-22 Proteins are thought to play a dominant role in this interaction due to their abundance, forming the protein corona.²³ Protein corona formation is a dynamic process, where high abundant-low affinity proteins can be replaced over time by low abundant-high affinity proteins.^{24,25} A "hard corona" describes the situation of high-affinity proteins irreversibly bound to the NP surface; conversely, a "soft corona" describes the situation of lower-affinity proteins that are reversibly bound to the NP surface or on top of hardcorona proteins.²⁶⁻²⁹ Clearly, then the bulk composition of a complex protein solution may not be the same as the composition of either the hard or soft protein coronas that surround nanoparticles in aqueous solution.

Most NP-protein corona complex studies are conducted using blood, cell culture medium with serum, a single protein, or a small mixture of proteins. More relevant are in vivo studies using intact living cells or whole organisms, which better reflect the thermodynamically and kinetically complex formation of protein coronas. ^{30–33} NMR has been introduced as a method to study protein corona formation in situ; however, mass spectrometry-based analysis is needed for more detailed molecular information, which requires NP-corona isolation.³⁴ Hence, new NP-corona isolation methods are necessary to further advance the field toward in vivo studies. Centrifugation, the standard method of NP-corona isolation, separates particles and proteins in the matrix based on difference in densities. 32,35 The method is harsh, however, and risks false identification of corona proteins. False positives may result from proteins/ protein complexes that did not bind to the NPs originally may sediment together with the NP-protein corona complexes during centrifugation process. False negatives may result from strong centrifugal forces causing protein dissociation. Magnetic separation, which requires magnetic NPs, offers a unique approach to isolate the NP-corona within an in vivo environment after administration.^{36–39} Though the use of magnetic NPs also comes with risks of agglomeration, it is thought to be a gentler isolation method compared to centrifugation.32

In this study, gold-coated iron oxide NPs are synthesized to take advantage of the magnetic cores for protein retrieval from biological systems. The gold coating provides the iron oxide cores with protection against oxidation and corrosion as well

[†]Department of Chemistry, University of Illinois at Urbana-Champaign, 600 S. Mathews Avenue, Urbana, Illinois, 61801, United State

[‡]Department of Chemistry and Biochemistry, Santa Clara University, 500 El Camino Real, Santa Clara, California, 95053, United States

^{*}To whom correspondence should be addressed: murphycj@illinois.edu

as ease of functionalization. The gold coating also equips the iron oxide NPs with optical properties, thanks to surface plasmon resonance, which will present unique route of characterizations, such as photoacoustic imaging. 40,41 An important path of NPs release into the environment is into the aquatic system, either during production, transport, or disposal, which motivates our choice of rainbow trout gill cells (RTgill-W1) as our biological system. Gills are a known target organ for NP uptake in fish, and the rainbow trout gill cell line is a model cell type for aquatic environment exposure. 42-44 To establish magnetic retrieval as a suitable method for cellular/organismal retrieval, gold-coated iron oxide NPs are first incubated with total protein extracts from the rainbow trout gill cells. The NPprotein corona complexes are retrieved magnetically and are compared to the NP-protein corona complexes retrieved by the conventional centrifugation method.

EXPERIMENTAL SECTION

Materials. Iron (III) chloride hexahydrate (FeCl₃·6H₂O), sodium acetate (NaCH3COO), ethylene glycol (anhydrous, 99.8%), branched polyethyleneimine (PEI) (MW~25,000 Da), tetrachloroauric (III) acid trihydrate (HAuCl₄·3H₂O) tetrakis(hydroxymethyl)phosphonium chloride (THPC) (80% solution in water), polyvinylpyrrolidone (PVP) (MW=40,000 Da), hydroxylamine hydrochloride (NH2OH·HCl), ammonium bicarbonate, and trypsin from bovine pancreas were purchased from Sigma-Aldrich. Trisodium citrate dihvdrate (Na₃C₆H₅O₇·2H₂O) was purchased from Flinn Scientific. Mammalian Protein Prep Kit (37901) was purchased from Oiagen. A PierceTM BCA protein assay kit and bovine serum albumin (BSA) standard were purchased from Thermo Scientific. All materials were used without further purification. A 100-ml Teflon-lined, stainless-steel autoclave purchased from Techinstro (AUTOCLAVE-PTFE-0110). RTgill-W1 trout gill cells were purchased from ATCC (CRL-2523TM).

Synthesis of PVP Au-coated iron oxide NPs. The nanoparticles were synthesized using a modified version of a procedure previously published by Wang et al.⁴⁵

Synthesis of iron oxide NPs. Iron oxide NPs of expected diameter 100 nm were synthesized via solvothermal as previously reported. He Briefly, 1.3 g FeCl₃·6H₂O, 0.52 g trisodium citrate, 2.4 g sodium acetate and 2.2 mL of H₂O were dissolved in 40 mL ethylene glycol in that order. The mixture was stirred vigorously for one hour before transferring to a 100-mL Teflon-lined, stainless-steel autoclave and heated to 200°C for 10 hours. The solid product was collected and washed with ethanol twice before drying under nitrogen.

NP functionalization with PEI. After the iron oxide NPs were dried, 50 mg of the powdered NPs were redispersed in 50 mL of 50 mg/mL aqueous PEI solution. After overnight incubation on a belly dancer shaker, the NPs were washed 3x at 500 xg for 30 min each time and redispersed into 50 mL DI water.

Synthesis of Au-seeded PEI-iron oxide NPs. Au-seeds were synthesized via THPC reduction⁴⁷ and stored in a refrigerator overnight before being incubated with the washed PEI-iron oxide NPs the next day. In typical procedure, 1 mL of PEI-iron oxide NPs was incubated with 49 mL of 2-3 nm Au seeds in a 50 mL centrifuge tube. After overnight incubation on a belly dancer shaker, the NPs were washed 3x at 500 xg for 30 mins each wash. After the last wash, the solid NP pellet was redispersed in 20 mL DI water.

Synthesis of PVP Au-coated iron oxide NPs. In a large batch synthesis, typically 600 mL of Au-seeded PEI-iron oxide NPs and 600 mL of DI water were added to a 2L Erlenmeyer flask. 12 g of PVP were added to the solution and the flask was mixed on a belly dancer shaker. When all the PVP was dissolved, 9 mL of 50 mg/mL NH₂OH·HCl was added to the solution. The flask was mixed manually before adding 9 mL of 1% w/v HAuCl₄·3H₂O. The solution turned brown to blue within minutes. The NPs were then washed once before drying under vacuum.

Nanoparticle characterization

Hydrodynamic light scattering and ζ-potential of the NPs were measured after each stage of synthesis using a Malvern Zetasizer Nano ZS. UV-Vis spectra and BCA assay readings were collected using an Agilent Technologies Cary 5000 UV-Vis-NIR. Transmission electron microscopy micrographs of the NPs in water were obtained by drop-casting onto copper grid with carbon type B 300 mesh (01813-F, Ted Pella) prior to imaging with a JEOL 2100 Cryo TEM with LaB₆ emitter operated at 200 keV. Elemental mapping analysis was conducted using FEI Themis Z operating at 300 keV with energy dispersive X-ray spectroscopy (EDS) system.

${\it Oncorhynchus\ mykiss\ rainbow\ trout\ gill\ (RTgill-W1)\ cell}$ culture

RTgill-W1 cells were cultured in L-15 medium supplemented with 10% FBS and 1% penicillin/streptomycin in T-75 and T-175 flasks in air at 19-20°C. The culture medium was replaced twice weekly, and cells were harvested for experiments and passage upon reaching 85-90% confluency. Adherent cells were removed from flasks by adding 0.25 % Trypsin-0.53 EDTA until cells detached (~5-10 mins). Cells used in subsequent experiments were from passages 3-10.

Total protein extraction and quantification

The total protein extraction was based on the Mammalian Protein Prep Kit (37901, Qiagen). Briefly, RTgill-W1 cells were seeded in T-75 or T-175 flasks until confluency and washed twice with ice cold PBS. The cells were removed by gentle scraping with cell-scraper after adding 10 mL ice cold PBS. The cells were then transferred to a centrifuge tube to pellet. The cell pellet (5-10 x 10⁶ cells) was then resuspended in lysis buffer with Benzonase® nuclease and protease inhibitor. The resuspended cells were incubated on a rotary shaker for 5 minutes at 4°C before centrifuging. The supernatant containing total protein extracts were then transferred to a new tube. The protein extracts were precipitated with cold acetone and redispersed in 10 mM NH₄HCO₃ pH= 8.

A Pierce™ BCA Protein Assay Kit (23225, Thermo Fisher) was used to quantify total protein concentration. Bovine serum albumin was used as standard for calibration curve.

Nanoparticle exposure to total protein extracts

PVP Au-coated iron oxide NPs were massed and dissolved in 10 mM NH₄HCO₃ at pH = 8 to make 1000 μ g/mL concentration in a 1 mL solution of 60 μ g/ml total protein extracts from RTgill-W1 cells. PVP Au-coated iron oxide NPs before and after incubating with protein extracts (1 hour, at 20°C) were characterized using dynamic light scattering. The NP-protein corona complexes were then isolated using a magnet or centrifugation once (1x) or twice (2x). BCA assays were used to quantify the amount of protein left in the supernatant after each wash. NP-protein corona complexes were then digested with trypsin (1:200 enzyme: protein) overnight at 37°C.

The NPs were removed by centrifugation and the protein coronas in the supernatants were analyzed using nanoLC-MS/MS.

Protein identification and relative quantitation by mass spectrometry

Briefly, samples were lyophilized and resuspended in 0.1 % trifluoroacetic acid (TFA) and cleaned with StageTips. The samples were then re-lyophilized and suspended in 0.1% FA/5% ACN for injection into UltiMate 3000 nanoLC and analyzed by Q Exactive HF-X high resolution mass spectrometer. The peptides were separated on a 25 cm long Aclaim Pepmap C18 column using 0.1% FA in water (mobile phase A) and 0.1% FA in 80% ACN (B) over the course of 90 minutes. Full MS scans from 350-1500 m/z were done at 120k in the Orbitrap, followed by high energy collision dissociation (HCD) of the 15 most abundant ions. MS2 scans were also analyzed in the Orbitrap with a resolution of 15k. Mass spectra were analyzed using the MaxQuant software version 2.0.1.0 containing the Andromeda search engine. The spectra were search against the Oncorhynchus mykiss (Rainbow Trout) UniProt sequence data base. Proteins were quantified using MaxLFQ, MaxQuant's implemented label free quantification (LFQ) algorithm, which bases on MS1 intensity. 48 Enzyme specificity was set to trypsin. The modifications of oxidation and N-terminal acetylation was included in protein quantification. Minimum peptide length of seven amino acids were allowed. A false discovery rate (FDR) of 1% was set for peptide and protein identifications. Protein identification required at least one unique or razor peptide per protein group. Contaminants, reverse counterparts, and proteins only identified with less than 2 unique peptides were excluded from further data analysis. The LFQ intensity data was log2-transformed and proteins that were sparsely quantified (those that do not have at least 2 valid values out of 3 replicates per condition) are removed. Missing values were imputed in Perseus software version 1.6.15.0, which uses random draws from a Gaussian distribution that were left shifted by 1.8 standard deviation and a width of 0.5.49 Molecular weight and gene ontology (cellular component) was extracted from UniProt database. Isoelectric point was calculated using Compute isoelectric point (pI) tool (https://web.expasy.org/compute pi/) and grand average of hydropathy (GRAVY) value was calculated using the GRAVY calculator (http://www.gravy-calculator.de).

RESULTS AND DISCUSSION

Synthesis and characterization of PVP Au-coated iron oxide NPs.

The iron oxide cores were first synthesized via a solvothermal reaction, producing materials with diameters ~100 nm, as measured by transmission electron microscopy (TEM). They are made of clusters of smaller primary nanocrystals (~4-10 nm) giving them a unique superparamagnetic property.⁴⁶ The citrate coating endows the NPs with a negatively charged surface (zeta potential -29 mV), which is then reversed after incubation with polyethyleneimine (PEI) to +44 mV. This positively charged surface allows the iron oxide NPs to interact electrostatically with negatively charged 2-3 nm gold seeds (synthesized via THPC reduction) that yield gold seeddecorated iron oxide NPs. These seeds were allowed to grow bigger and intersect, forming a gold coating around the iron oxide core and were ultimately capped with polyvinylpyrrolidone (PVP). The final PVP Au-coated iron oxide NPs are ~150 nm in size as measured by TEM, with the hydrodynamic diameter of ~200 nm with a slightly negative zeta potential of ~-15 mV. Figure 1 shows TEM micrographs of the NPs as they grow from the original ~100 nm iron oxide NPs (Figure 1A) to Au-seeded iron oxide NPs (Figure 1B) to ~150 nm Aucoated iron oxide NPs (Figure 1C). Elemental mapping conducted using energy dispersive X-ray spectroscopy in scanning transmission electron microscopy (STEM-EDS) shown in Figure 1D confirms the core- shell structure. As observed in TEM images, the gold shell is made up of cluster aggregates of AuNPs.

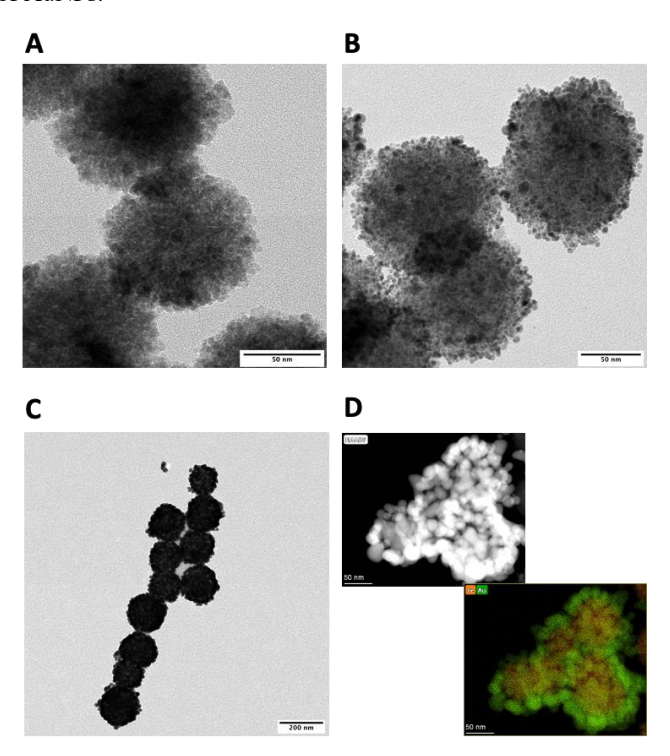


Figure 1. Representative TEM micrographs for (A) iron oxide NPs (scale bar = 50 nm) (B) Au-seeded iron oxide NPs (scale bar = 50 nm) (C) Au-coated iron oxide NPs (scale bar = 200 nm) and STEM-EDS maps for (D) Au-coated iron oxide NPs showing core-shell structure (Au-green, Fe-orange, scale bar = 50 nm).

Quantification of retrieved protein corona via magnet and centrifugation from incubation with total protein extracts.

Adherent RTgill-W1 cells were grown in L-15 medium with 10% FBS and penicillin/streptomycin to 85-90% confluency before being lysed for total protein extraction. The total protein extracts (60 µg/mL) were then incubated with 1 mg/mL PVP-Au-coated iron oxide NPs for 1 hour at 20°C. The NPs before and after protein incubation were characterized using dynamic light scattering and ζ-potential analysis to infer protein corona formation. As seen in Figure 2A, the hydrodynamic diameter of NPs increases from ~200 nm to ~290 nm after protein incubation, indicating protein adsorption to the surface in a multilayer fashion. The binding interaction is also inferred in the increased negative ζ-potential in Figure 2B. The NPprotein complex pellets were then retrieved either with a magnet (15 minutes) or by centrifugation (1,000 xg, 15 minutes) followed by washing with water either once (1x) or twice (2x) as illustrated in Figure S1. The hydrodynamic diameter of the NPs increased significantly after washing steps, suggesting NP agglomeration as opposed to increasing protein corona content.⁵⁰ The supernatant and the pellet (NPs + protein corona complexes) were analyzed using a colorimetric BCA assay to quantify the amount of protein in all compartments (Figure 3).

As seen in Figures 2A and 3, while there is no significant difference between the hydrodynamic diameter of magnetically retrieved and centrifuged samples (for both washes), there is a significant difference in the concentration of protein in the supernatant between the magnet 1x (M1) and centrifuged 1x (C1) samples (unpaired t-test, p = 0.0009) and a significant difference in the concentration of protein the pellet between the M1 and C1 samples (unpaired t-test, p = 0.0484). A similar trend can be seen in the second wash; however, the difference was not significant by the t-test. This result indicates that the centrifugation method isolates larger amounts of protein compared to magnetic retrieval. Some losses of total protein occur in all processing steps, compared to the original protein extract (Figure 3).

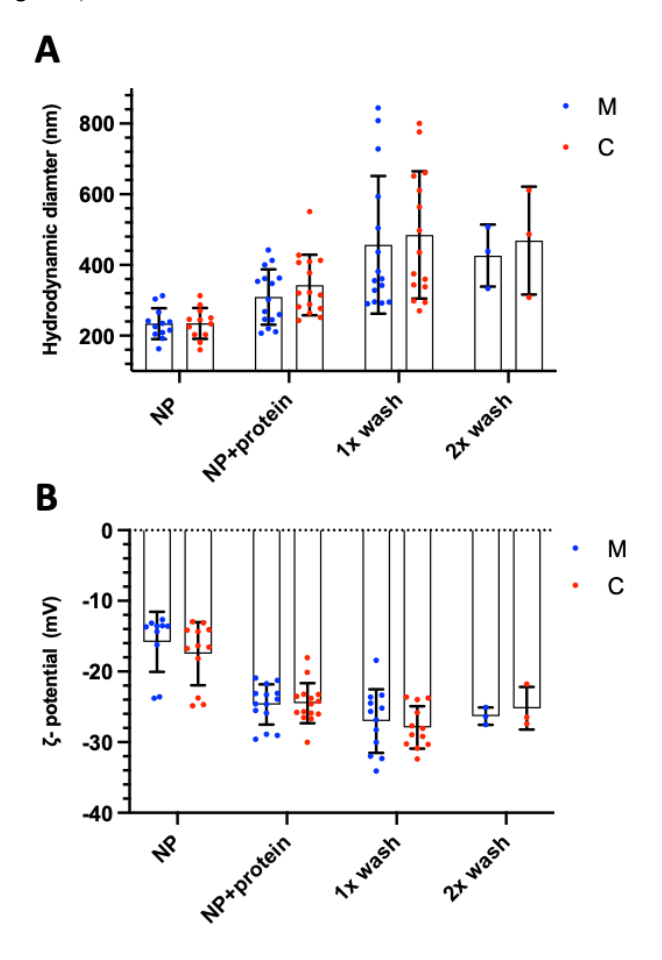


Figure 2. (A) Hydrodynamic diameter and (B) ζ -potential measurements of Au-coated iron oxide NPs before, after incubation with total protein extracts, and after washes after either magnetic retrieval (blue) or centrifugation (red). Each point represents a replicate obtained by averaging 4 measurements for hydrodynamic diameter. Error bars represent standard deviation.

Qualitative proteomic results show protein enrichment dependent on the isolation method.

In addition to comparing the amount of protein retrieved by the two isolation methods, protein identification was performed. The NP-protein corona complexes retrieved either by a magnet (M) or centrifugation (C) after 1x wash or 2x wash were digested with trypsin (1:200 enzyme: protein by mass) overnight at 37°C. The NPs were then removed by centrifugation in all samples. The original protein extract was also trypsinized. The samples were then analyzed by nanoLC-

MS/MS.⁵¹ The mass measurements for intact peptide and MS/MS fragments were matched to theoretical sequences using Mascot search engine and searched against the *Oncorhynchus mykiss* proteome. Only protein hits found in all 6 replicates for all conditions (5 for magnet samples) were considered for further qualitative analysis.

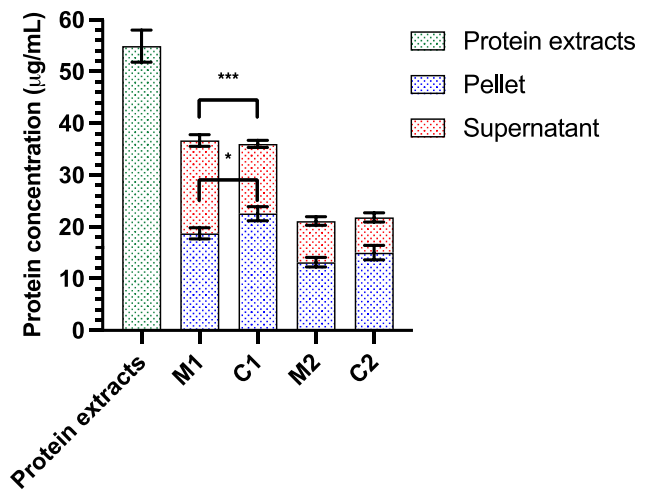


Figure 3. Total protein quantification as function of processing steps for the original protein extracts (green), and for NP-containing pellets (blue) and supernatants (red) after separation via magnet retrieval or centrifugation after one wash (1x wash; M1, C1) or two washes (2x wash; M2, C2). Error bars represent the error of the mean from at least 7 replicates. Asterisks correspond to the following p values using unpaired t-test, * p<0.05, *** p<0.001.

Proteins found in magnetically-retrieved and centrifuged samples after the first wash are compared to each other and to the proteins found in the protein extracts in absence of NPs, as seen in Figure 4. Proteins found in magnetically-retrieved and centrifuged samples after the first wash are compared to each other and to the proteins found in the protein extracts in absence of NPs, as seen in Figure 4A. Of the 356 proteins identified in M1 samples, 45.5% are also identified in C1 and PE samples; whereas 18.8% are shared with C1 samples only, 10.4% are shared with PE samples only, and 25.3% are uniquely identified in M1 samples. Similarly, out of the 300 proteins identified in M2 samples, 47.7 % are shared with in C2 and PE samples; whereas 21.3% are shared with C2 samples only, 12.7% are shared with PE samples alone, and 18.3% are uniquely identified in M2 samples (figure 4B). A grand comparison among all samples is presented in Figure 4C, which qualitatively shows universal proteins found in all sample types as well as uniquely found proteins in each sample type. These results show that the isolation method and the number of washes bias the protein corona composition.

Relative quantitative proteomic results show differences between protein corona isolated magnetically compared to centrifugation.

To gain a more detailed understanding of how the isolation method affects protein corona composition, we identified and quantified proteins using label-free quantitative nanoLC-MS/MS. The samples were prepared in a similar manner as those in the qualitative analysis, but this time the fragmented proteins were quantified by the BCA assay before injection to ensure the same amount of protein was injected for each sample for relative comparison. Since the efficiency of the ioniza-

tion process can differ by order of magnitude for different peptides, the number of detected ions of the intact (precursor) peptide, reflected in the integrated MS1 intensity, is not a good readout for absolute amount of peptide in the samples; however, this integrated MS1 intensity can be used for relative quantification for the same peptide in different samples.^{51,52} The MaxLFQ algorithm, integrated in the MaxQuant software, was used to construct a triangular matrix containing all pairwise protein ratios between any two samples and perform a least-squares analysis to reconstruct the abundance profile that satisfies the individual protein ratios, reported as LFO (labelfree quantitative) intensity.⁴⁸ Peptide and fragment masses were searched against the Oncorhynchus mykiss proteome using the Andromeda search engine within MaxQuant. Since the database search not only includes target sequences, but also their reverse counterparts and possible contaminants, these hits are removed along with proteins that were identified by less than 2 unique peptides. These protein intensities were then log₂-transformed to obtain a normal distribution of the protein intensities in the sample. Those proteins that were quantified will become invalid after log₂transformation since their LFQ intensity measurements were 0. Only proteins with at least 2 valid values in each condition were kept for further analysis. Those missing values are imputed with numbers that are considered "small" in each sample by drawing from a normal distribution with a mean that is downshifted from the sample mean (1.8) and a standard deviation that is a fraction of the sample distribution (0.5).

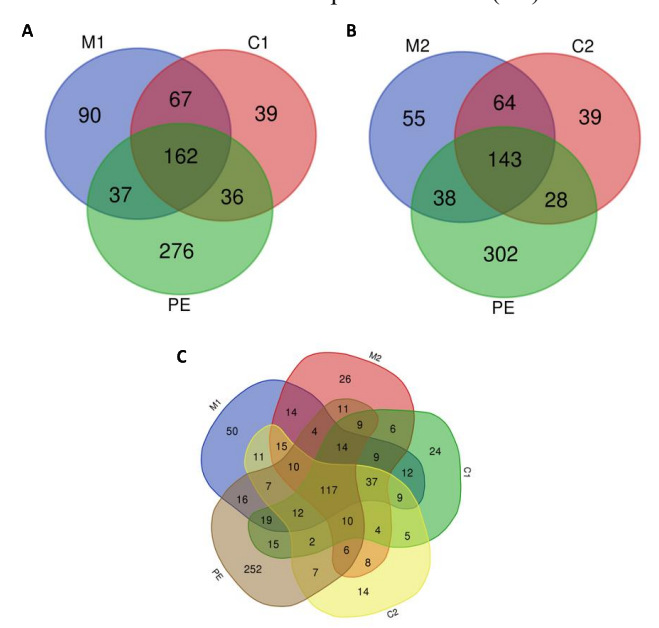


Figure 4. Venn diagrams comparing qualitative protein hits found among NP samples. (A) NP-protein pellets isolated via magnet retrieval after one wash (M1) in blue, isolated by centrifugation after one wash (C1) in red, and original protein extract (PE) in green. (B) NP-protein pellets isolated via magnet retrieval after two washes (M2) in blue, isolated by centrifugation after two washes (C2) in red, and original protein extract (PE) in green. (C) A grand comparison of proteins found in common and unique to M1, M2, C1, C2, and original protein extract (PE).

The filtered list of quantified proteins consists of 1766 proteins. To be considered significant, our threshold is that the difference in log₂(LFQ intensity) between the samples being compared must be at least 1, representing at least 2-fold change. When a protein has significantly higher abundance in

"on particle" samples (M1, M2, C1, C2) compared to protein extracts (PE) samples, we consider this protein as enriched on the NPs' surface. On the other hand, when a protein has significantly higher abundance in PE samples compared to "on particle" samples (M1, M2, C1, C2), this protein is considered not enriched on the NPs' surface. The visual representation for these types of proteins is presented in Figure S2A and S2B. Heat maps for the proteins that are considered enriched on the NPs' surface are shown in Figure S3A and for those that are not enriched on the NPs' surface are shown in Figure S3B. Interestingly, as seen in Figure 5A there are proteins that have significantly higher abundance in magnet samples (M1, M2) compared to PE samples, while their abundance in centrifuged samples (C1,C2) is not significantly different compared to PE samples, and vice versa. The visual representation for these types of proteins is presented in Figure S2C and S2D. The heat maps for these proteins are shown in Figure S4A and S4B. Biophysiochemical properties of those proteins that are enriched are compared to those that are not enriched on the NP's surface in terms of molecular weight, hydrophobicity, pI, and cellular components (Figure S5A-C). Proteins that are enriched on the NPs' surface in both M and C samples have greater prevalence for high molecular weight, hydrophilic, and positively charged proteins. Given the negatively-charged surface of these hydrophilic NPs, the enrichment of hydrophilic and positively-charged proteins is understandable and in agreement with previous studies.53-55 Biophysiochemical properties of those proteins that are enriched on M samples only is also compared to those proteins that are enriched on C only. Although there is no significant difference in terms of molecular weight, hydrophobicity, and pI, there are differences in cellular component distributions between the two lists of proteins (Figure S6A-C). These results highlight the difference between magnetization and centrifugation as a protein corona isolation method.

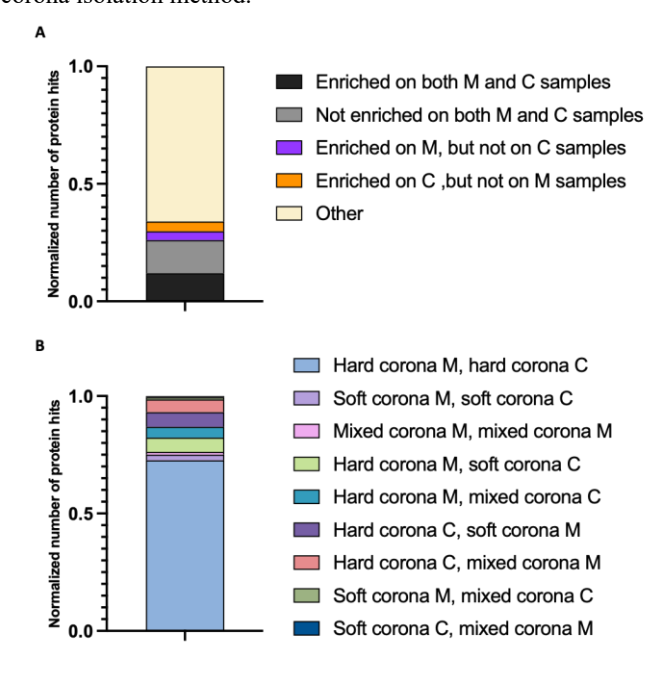
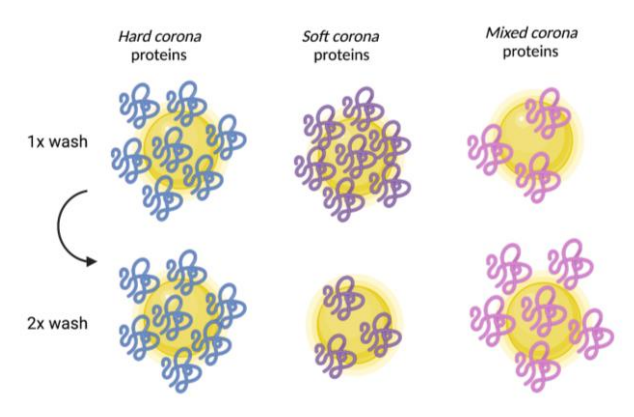


Figure 5. The 1766 quantified proteins are categorized based on their log₂(LFQ intensity) and normalized (A) On-particle samples (M1, M2, C1, C2) in comparison to PE samples (B) M1 in comparison to M2 and C1 in comparison to C2.

We also identified proteins whose abundance level is stable across washes ($\Delta(\log_2(\text{LFQ intensity}) < 1)$), which we call *hard*

corona proteins. We call the proteins whose relative abundances decrease significantly with increasing number of washes soft corona proteins due to their inferred lower binding affinity compared to the hard corona proteins. There are also proteins whose relative abundances significantly increase with increasing number of washes. These proteins are being enriched after the second wash, which could have been part of the hard or soft corona; hence, we call them mixed corona. The visual representation for these types of proteins is presented in Scheme 1, illustrating the change in the relative abundance after the first and second washes. One way to think about mixed corona proteins is that their abundance depends on sample history; they may be out-competed for NP binding at one stage in the separation process but then successfully recompete at a later stage. In the literature, the majority of hard protein corona studies involve isolation of NPs from the biological media employing at least 3 washing steps to ensure removal of unbound proteins from the original biological fluid. 56,57 Hence, our washing steps might be considered insufficient; however, as seen in figure S7, we were still able to identified hard, soft and mixed corona proteins in both magnet and centrifuged samples that have abundances significantly different from the PE samples. As seen in Figure 5B, there are proteins that are considered part of the hard corona, soft corona, or *mixed corona* in both M and C samples; however, there are also proteins that are considered the hard corona in M samples but is considered soft corona in the C samples (and vice versa), or those that are considered *hard corona* in M samples but is considered mixed corona in the C samples (and vice versa), or those that are considered *soft corona* in M samples but is considered *mixed corona* in C samples (and vice versa). The visual representations for these types of proteins are presented in Figure S8.

Scheme 1. *Hard corona* proteins are stable to second washes; *soft corona* proteins are lost in the second wash; and *mixed corona* proteins are unusual in that they are more abundant in the second wash compared to the first wash.



The heatmaps for the proteins that are considered *hard*, *soft*, or *mixed corona* in both M and C samples are presented in Figure S9. These proteins are then furthered analyzed by comparing their log₂(LFQ intensity) values to the corresponding values in the PE samples. We observed that there are more proteins that are considered enriched on the NPs' surface in the *hard corona* proteins, whereas there are more proteins that are considered not enriched on the NPs' surface in the *soft* and *mixed corona* (Figure S10). This result is not surprising since *hard corona* proteins have high binding affinity to the NPs' surface, hence allowing them to be detected at a higher abundance compared to PE samples. Whereas, *soft* or *mixed* corona

differ in binding affinity and exchanging rate, hence they are not detected at a higher abundance compared to PE samples. When comparing the log₂(LFQ intensity) values of these proteins in the M samples compared to the C samples, as shown in Figure S11, we observed that there are more proteins with higher relative abundance isolated by centrifugation compared to magnetization. This result supports the BCA results in Figure 3, which showed that larger amounts of proteins are isolated with centrifugation. We also investigated the difference in the degree of washing in M and C samples for soft and mixed corona proteins, as shown in Figure 6. The change in log₂(LFQ intensity) from 1x wash to 2x wash for soft corona proteins in centrifuged samples is significantly higher than in magnet samples (unpaired t-test, p = 0.00249) (Figure 6A). This shows that centrifugation is removing these *soft corona* proteins more effectively compared to magnetization. The change in log₂(LFQ intensity) from 2x to 1x for mixed corona proteins are presented in Figure 6B, where there is no significant difference between centrifuged samples compared to magnet samples.

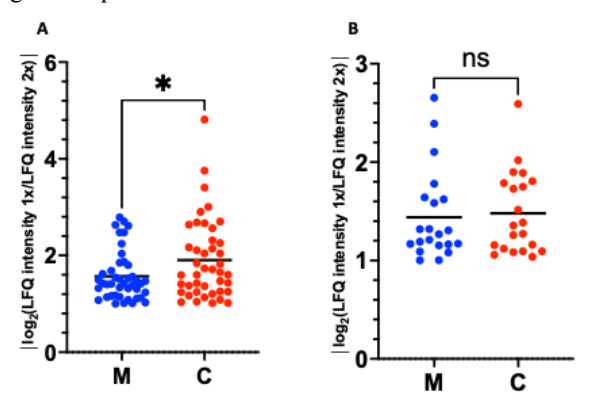


Figure 6. The change in log₂(LFQ intensity) between washes of M and C samples that are A) *soft corona* proteins, and B) *mixed corona* proteins. Each point corresponds to a single protein hit. * p<0.05 using unpaired t-test.

The presence of those proteins that are considered part of hard corona in M samples but soft corona in C samples (and vice versa) or those that are considered part of the hard corona in M samples but *mixed corona* in C samples (and vice versa) highlight the discrepancy between the two isolation methods (Figure 5B, S8A-B, S12A-D). If the two isolation methods were equivalent, those proteins that are considered hard corona in M samples should also be considered hard corona in C samples and so forth. We also compared the relative abundance of these proteins to the corresponding abundance in the PE samples and observed that there are more "not enriched on NPs' surface" proteins than "enriched on NPs' surface." This result again shows that hard corona proteins are more likely to be "enriched on the NPs' surface," while soft or mixed corona proteins are more likely to be "not enriched on the NPs" surface." To further interrogate the isolation method bias, these lists of proteins were also examined in terms of molecular weight, hydrophobicity, pI, and cellular component, as shown in Figure 7A-D. Low molecular weight proteins (<10 kDa) are only detected in the list of proteins that are hard corona in M (C) but soft corona in C (M) samples and not on the list of proteins that are hard corona in M (C) but mixed corona in C (M) (Figure 7A). The percentage of hydrophobic proteins decreases when comparing between the list of hard corona M, soft corona C and hard corona M, mixed corona C. On the

other hand, the percentage of hydrophobic proteins increases when comparing between the list of hard corona C, soft corona M and hard corona C, mixed corona M (Figure 7B). Interestingly, the percentage of positively-charged proteins decreases when comparing between the list of hard corona M, soft corona C and hard corona M, mixed corona C. On the other hand, the percentage of positively-charged proteins increases when comparing between the list of hard corona C, soft corona M and hard corona C, mixed corona M (Figure 7C). The reversed trend between the lists of hard corona in M (C) while soft corona in C (M) proteins and the list of hard corona in M (C) while mixed corona in C (M) proteins shows that the nature of the proteins being removed is different in comparison to those being enriched. This result suggests that the protein corona is multilayer, and the when the proteins that are considered soft corona are removed, other proteins are either recruited to the NPs' surface or are now uncovered to be more accessible to be digested and detected, hence increased

relative abundance, or being part of the *mixed corona*. When comparing between proteins that are hard corona M, soft corona C and hard corona C, soft corona M, we also observed that centrifugation removes higher percentage of positively charged proteins than magnetization and magnetization removes higher percentage of hydrophilic proteins than centrifugation. This suggests that centrifugal force overcomes electrostatic attraction forces to remove more positively-charged proteins from the negatively-charge NPs' surface while magnetic force overcomes van deer Waals attraction forces to remove more hydrophilic proteins from the hydrophilic NP's surface. Figure 7D shows the diverse in the distribution of these protein lists in terms of cellular components. Membrane, mitochondria, cytoplasm, and nucleus proteins can be found in all the lists, but there are also proteins of unique cellular component that can only be found in one of the four lists of proteins.

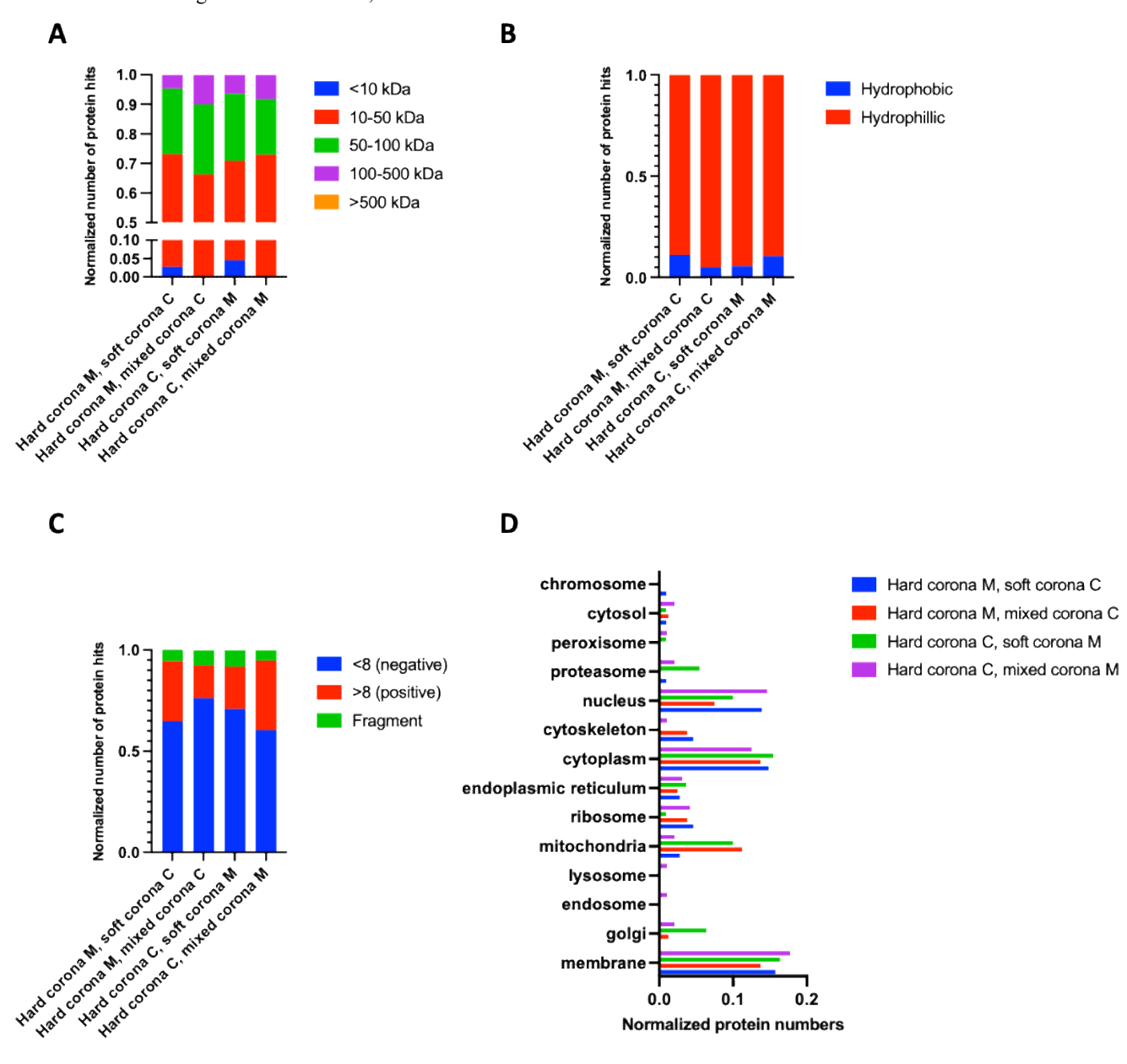


Figure 7. Comparison of the biophysiochemical properties of the proteins in the *hard corona* of magnetically retrieved samples while being in the *soft corona* of centrifuged samples and vice versa; proteins in the *soft corona* of magnetically retrieved samples while being in

the *mixed corona* of centrifuged samples and vice versa. (A) Distribution of proteins based on molecular weight range (B) Distribution of proteins based on hydrophobicity (C) Distribution of proteins based on pI (D) distribution of proteins based on cellular components.

We also compared the change in relative abundance between washes of the proteins that are considered soft corona proteins in M samples (while considered hard corona proteins in the C samples) to the change in relative abundance between washes of the proteins that are considered soft corona proteins in C samples (while considered hard corona proteins in M samples) as shown in Figure 8A. Similar to when the proteins' abundance was decreasing in both samples types in Figure 6A, we also observed that centrifugation is removing the proteins at a significantly higher extent compared to centrifugation (unpaired t-test, p = 0.0167). The comparison between the change in relative abundance between washes of the proteins that are considered *mixed corona* proteins in the M samples (while considered hard corona proteins in the C samples) and the proteins that are considered *mixed corona* proteins in C samples (while being considered hard corona proteins in M samples) is shown in Figure 8B. Similar to when the proteins' abundance was increasing in both sample types in Figure 6B, magnetization and centrifugation enrich the proteins to a similar extent.

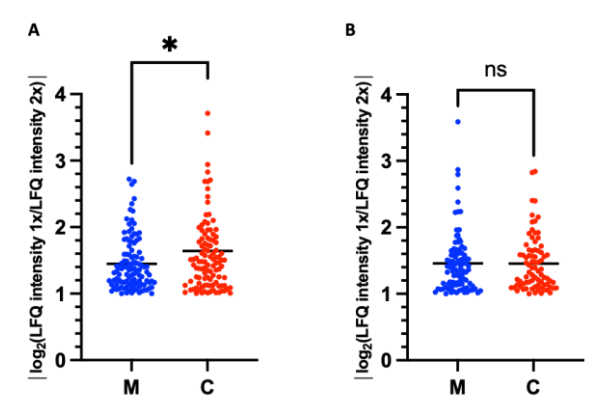


Figure 8. The change in log₂(LFQ intensity) between washes of (A) *soft corona* proteins in M samples (*hard* in C samples) and *soft corona* proteins in C samples (*hard* in M samples) (B) *mixed corona* proteins in M samples (*hard* in C samples) and *mixed* corona proteins in C samples (hard in M samples). Each point corresponds to a single protein hit. * p<0.05 using unpaired t-test.

We also identified proteins that are soft corona proteins in M samples but *mixed corona* in C samples and those that are soft corona proteins in C samples but mixed corona in M samples (Figure 5B, S8C). As seen in Figure S13A-B, the extent of removing and enriching between the two isolation methods are quite similar. The biophysiochemical properties of these proteins are also examine further in terms of molecular weight, hydrophobicity, pI, and cellular components (Figure S14A-D). There is no obvious distinction in molecular weight, hydrophobicity, nor pI to explain the bias of the isolation method. Cellular component distribution does shows that there is a preference for nucleus and membrane proteins to be removed (soft corona) by centrifugation and enriched (mixed corona) by magnetization, and preference for cytosol, proteasome, cytoplasm, endoplasmic reticulum, and mitochondria to be removed (soft corona) by magnetization and enriched (mixed corona) by centrifugation (Figure S14D).

Chan et al. recently showed that proteins organize themselves into assembly-like structures through protein-protein interactions coating the NPs in multilayered protein corona structure, where the foundational protein corona layer interacts directly with the NPs surface likely dependent on the NPs chemical composition and surface chemistries, which in turns governs the subsequent protein adsorption.⁵⁸ The strong protein-protein interactions can be observed with our results, where washing steps and isolation methods preferably remove or enrich different proteins, changing the organization of proteins within the corona. This show that isolation methods can be used to manipulate the downstream biological effects, but they can also be modifying the protein corona composition. Prediction of such effects could be gained by binding affinity studies of individual proteins to NPs, which for cell extract samples like ours would be non-trivial. We also compared the proteins identified in our samples to the proteins identified by Schirmer et al⁴² that were isolated using centrifugation once after incubating 20 nm silver NPs with trout gill cell protein extracts. ADF-H domain-containing protein, GST class-pi, and pyruvate kinase as part of the hard corona proteins found in both of our M and C samples were also found in their list of proteins, which are all on the top 20 most abundance proteins found in our PE samples. We also identified malic enzyme, protein RER1, and protein disulfide-isomerase as part of the soft corona proteins found in both of our M and C samples that are also found in the protein corona by Schirmer et al. These soft corona proteins: however, are not in the top 20 most abundance proteins found in our PE samples. We did not identify any shared proteins between our mixed corona proteins in both M and C samples and proteins identified by Schirmer et al. These overlaps show that these proteins might be interesting to manipulate and control the biological identity of the NPs.

CONCLUSIONS

Au-coated iron oxide NPs were incubated with rainbow trout gill cell total protein extracts before retrieval with either a magnet or centrifugation to analyze the NP-protein corona complexes. Although there is no significant difference in the hydrodynamic diameter of the NP-protein corona complexes after magnetic isolation or centrifugation, centrifugation isolates higher amount of proteins in the pellet compared to magnetization. By examining relative abundance of proteins with increasing number of washes, we were able to identify proteins that are in the hard corona, soft corona, or mixed corona in both magnet and centrifuged samples, as well as those that are biased by the isolation method. We infer that centrifugal force overcomes electrostatic attraction forces to remove more positively-charged proteins while magnetic force overcomes van der Waals attraction forces to remove more hydrophilic proteins. We also see that centrifugation removes proteins at a higher extent compared to magnetization while the two isolation methods enrich proteins in a similar manner. This work highlights the role of isolation methods on determining the protein corona composition, which should be taken into consideration when design protein corona analysis experiments.

ASSOCIATED CONTENT

Supporting Information

The Supporting Information is available free of charge on the ACS Publications website.

Scheme of sample processing, visual representations of hard, soft, and mixed corona protein in M and C sam-

ples, heat maps and biophysiochemical properties of proteins mentioned in the text (PDF)
List of proteins and their characteristics (XLSX)

AUTHOR INFORMATION

Corresponding Author

Catherine J. Murphy* - Department of Chemistry, University of Illinois at Urbana- Champaign, 600 S Mathews Avenue, Urbana, IL 61801, United States; email: murphycj@illinois.edu; ORCID: 0000-0001-7066-5575

Authors

Khoi Nguyen L. Hoang - Department of Chemistry, University of Illinois at Urbana- Champaign, 600 S Mathews Avenue, Urbana, IL 61801, United States; email: klhoang2@illinois.edu; ORCID: 0000-0002-3822-4216

Korin E. Wheeler – Department of Chemistry and Biochemistry, Santa Clara University, 500 El Camino Real, Santa Clara, CA 95053, United States; email: kwheeler@scu.edu; ORCID: 0000-0002-4711-5062

Author Contributions

C.J.M. directed the research, which was performed by K. N. L. H. K.E.W. assisted in data analysis and interpretation. All authors contributed to the writing of the manuscript.

ACKNOWLEDGMENT

This material is based upon work supported by the National Science Foundation under Grant No. CHE-2001611, the NSF Center for Sustainable Nanotechnology (CSN). The CSN is part of the Centers for Chemical Innovation Program. Electron microscopy was carried out at the Frederick Seitz Materials Research Laboratory Central Research Facilities, University of Illinois at Urbana-Champaign. We would like to thank Dr. Sandy McMasters at the Cell Media Facility, University of Illinois at Urbana-Champaign for the help with cell culture media preparation and Dr. Justine Arrington at the Protein Sciences Facility of Roy J. Carver Biotechnology Center, University of Illinois at Urbana-Champaign for the raw proteomic data. Illustrations are created with BioRender.com

REFERENCES

- Maurer-Jones, M. A.; Gunsolus, I. L.; Murphy, C. J.; Haynes, C. L. Toxicity of Engineered Nanoparticles in the Environment. Anal. Chem. 2013, 85 (6), 3036–3049. https://doi.org/10.1021/ac303636s.
- (2) Ali, M. R. K.; Wu, Y.; Tang, Y.; Xiao, H.; Chen, K.; Han, T.; Fang, N.; Wu, R.; El-Sayed, M. A. Targeting Cancer Cell Integrins Using Gold Nanorods in Photothermal Therapy Inhibits Migration through Affecting Cytoskeletal Proteins. Proc. Natl. Acad. Sci. U. S. A. 2017, 114 (28), E5655–E5663. https://doi.org/10.1073/pnas.1703151114.
- (3) Rastinehad, A. R.; Anastos, H.; Wajswol, E.; Winoker, J. S.; Sfakianos, J. P.; Doppalapudi, S. K.; Carrick, M. R.; Knauer, C. J.; Taouli, B.; Lewis, S. C.; Tewari, A. K.; Schwartz, J. A.; Canfield, S. E.; George, A. K.; West, J. L.; Halas, N. J. Gold Nanoshell-Localized Photothermal Ablation of Prostate Tumors in a Clinical Pilot Device Study. *Proc. Natl. Acad. Sci. U. S. A.* 2019, 116 (37), 18590–18596. https://doi.org/10.1073/pnas.1906929116.
- (4) Mitchell, M. J.; Billingsley, M. M.; Haley, R. M.; Wechsler, M. E.; Peppas, N. A.; Langer, R. Engineering Precision Nanoparticles for Drug Delivery. *Nat. Rev. Drug Discov.* 2021, 20 (2), 101–124. https://doi.org/10.1038/s41573-020-0090-8.
- (5) Smith, B. R.; Gambhir, S. S. Nanomaterials for in Vivo Imaging. *Chem. Rev.* 2017, 117 (3), 901–986. https://doi.org/10.1021/acs.chemrev.6b00073.
- (6) Huang, P. C.; Chaney, E. J.; Aksamitiene, E.; Barkalifa, R.; Spillman, D. R.; Bogan, B. J.; Boppart, S. A. Biomechanical Sensing of in Vivo Magnetic Nanoparticle Hyperthermia-Treated Melanoma Using Magnetomotive Optical Coherence

- Elastography. *Theranostics* **2021**, *11* (12), 5620–5633. https://doi.org/10.7150/thno.55333.
- (7) Alafeef, M.; Dighe, K.; Moitra, P.; Pan, D. Rapid, Ultrasensitive, and Quantitative Detection of SARS-CoV-2 Using Antisense Oligonucleotides Directed Electrochemical Biosensor Chip. ACS Nano 2020, 14 (12), 17028–17045. https://doi.org/10.1021/acsnano.0c06392.
- (8) Qiu, T. A.; Guidolin, V.; Hoang, K. N. L.; Pho, T.; Carra', A.; Villalta, P. W.; He, J.; Yao, X.; Hamers, R. J.; Balbo, S.; Feng, Z. V.; Haynes, C. L. Nanoscale Battery Cathode Materials Induce DNA Damage in Bacteria. *Chem. Sci.* 2020, 11 (41), 11244–11258. https://doi.org/10.1039/d0sc02987d.
- (9) Niemuth, N. J.; Curtis, B. J.; Hang, M. N.; Gallagher, M. J.; Fairbrother, D. H.; Hamers, R. J.; Klaper, R. D. Next-Generation Complex Metal Oxide Nanomaterials Negatively Impact Growth and Development in the Benthic Invertebrate Chironomus Riparius upon Settling. *Environ. Sci. Technol.* 2019, 53 (7), 3860–3870. https://doi.org/10.1021/acs.est.8b06804.
- (10) Geppert, M.; Sigg, L.; Schirmer, K. Toxicity and Translocation of Ag, CuO, ZnO and TiO2nanoparticles upon Exposure to Fish Intestinal Epithelial Cells. *Environ. Sci. Nano* **2021**, *8* (8), 2249–2260. https://doi.org/10.1039/d1en00050k.
- (11) Kakakhel, M. A.; Wu, F.; Sajjad, W.; Zhang, Q.; Khan, I.; Ullah, K.; Wang, W. Long-Term Exposure to High-Concentration Silver Nanoparticles Induced Toxicity, Fatality, Bioaccumulation, and Histological Alteration in Fish (Cyprinus Carpio). Environ. Sci. Eur. 2021, 33 (1). https://doi.org/10.1186/s12302-021-00453-7.
- (12) Bogart, L. K.; Pourroy, G.; Murphy, C. J.; Puntes, V.; Pellegrino, T.; Rosenblum, D.; Peer, D.; Lévy, R. Nanoparticles for Imaging, Sensing, and Therapeutic Intervention. *ACS Nano* **2014**, *8* (4), 3107–3122. https://doi.org/10.1021/nn500962q.
- (13) Murphy, C. J.; Vartanian, A. M.; Geiger, F. M.; Hamers, R. J.; Pedersen, J.; Cui, Q.; Haynes, C. L.; Carlson, E. E.; Hernandez, R.; Klaper, R. D.; Orr, G.; Rosenzweig, Z. Biological Responses to Engineered Nanomaterials: Needs for the next Decade. ACS Cent. Sci. 2015, 1 (3), 117–123. https://doi.org/10.1021/acscentsci.5b00182.
- (14) Masciangioli, T.; Zhang, W. X. Environmental Technologies at the Nanoscale. *Environ. Sci. Technol.* 2003, 37 (5). https://doi.org/10.1021/es0323998.
- Ge, C.; Tian, J.; Zhao, Y.; Chen, C.; Zhou, R.; Chai, Z. Towards Understanding of Nanoparticle–Protein Corona. *Arch. Toxicol.* 2015, 89 (4), 519–539. https://doi.org/10.1007/s00204-015-1458-0.
- (16) Wheeler, K. E.; Chetwynd, A. J.; Fahy, K. M.; Hong, B. S.; Tochihuitl, J. A.; Foster, L. A.; Lynch, I. Environmental Dimensions of the Protein Corona. *Nat. Nanotechnol.* 2021, 16 (6), 617–629. https://doi.org/10.1038/s41565-021-00924-1.
- (17) Salvati, A.; Pitek, A. S.; Monopoli, M. P.; Prapainop, K.; Bombelli, F. B.; Hristov, D. R.; Kelly, P. M.; Åberg, C.; Mahon, E.; Dawson, K. A. Transferrin-Functionalized Nanoparticles Lose Their Targeting Capabilities When a Biomolecule Corona Adsorbs on the Surface. *Nat. Nanotechnol.* 2013, 8 (2), 137–143. https://doi.org/10.1038/nnano.2012.237.
- (18) Fleischer, C. C.; Payne, C. K. Secondary Structure of Corona Proteins Determines the Cell Surface Receptors Used by Nanoparticles. *J. Phys. Chem. B* **2014**, *118* (49), 14017–14026. https://doi.org/10.1021/jp502624n.
- (19) Zhang, X.; Pandiakumar, A. K.; Hamers, R. J.; Murphy, C. J. Quantification of Lipid Corona Formation on Colloidal Nanoparticles from Lipid Vesicles. *Anal. Chem.* 2018, 90 (24), 14387–14394. https://doi.org/10.1021/acs.analchem.8b03911.
- (20) Lima, T.; Bernfur, K.; Vilanova, M.; Cedervall, T. Understanding the Lipid and Protein Corona Formation on Different Sized Polymeric Nanoparticles. *Sci. Rep.* **2020**, *10* (1), 1–9. https://doi.org/10.1038/s41598-020-57943-6.
- (21) Griffith, D. M.; Jayaram, D. T.; Spencer, D. M.; Pisetsky, D. S.; Payne, C. K. DNA-Nanoparticle Interactions: Formation of a DNA Corona and Its Effects on a Protein Corona. *Biointerphases* **2020**, *15* (5), 051006. https://doi.org/10.1116/6.0000439.
- (22) Pink, M.; Verma, N.; Kersch, C.; Schmitz-Spanke, S. Identification and Characterization of Small Organic Compounds within the Corona Formed around Engineered Nanoparticles. *Environ. Sci. Nano* 2018, 5 (6), 1420–1427.

- https://doi.org/10.1039/c8en00161h.
- (23) Monopoli, M. P.; Walczyk, D.; Campbell, A.; Elia, G.; Lynch, I.; Baldelli Bombelli, F.; Dawson, K. A. Physical-Chemical Aspects of Protein Corona: Relevance to in Vitro and in Vivo Biological Impacts of Nanoparticles. J. Am. Chem. Soc. 2011, 133 (8), 2525–2534. https://doi.org/10.1021/ja107583h.
- (24) Vroman, L.; Adams, A. L. Identification of Rapid Changes at Plasma–Solid Interfaces. J. Biomed. Mater. Res. 1969, 3 (1), 43–67. https://doi.org/10.1002/jbm.820030106.
- (25) Casals, E.; Pfaller, T.; Duschl, A.; Oostingh, G. J.; Puntes, V. Time Evolution of the Nanoparticle Protein Corona. ACS Nano 2010, 4 (7), 3623–3632. https://doi.org/10.1021/nn901372t.
- (26) Walkey, C. D.; Chan, W. C. W. Understanding and Controlling the Interaction of Nanomaterials with Proteins in a Physiological Environment. *Chem. Soc. Rev.* **2012**, *41* (7), 2780–2799. https://doi.org/10.1039/c1cs15233e.
- (27) Monopoli, M. P.; Åberg, C.; Salvati, A.; Dawson, K. A. Biomolecular Coronas Provide the Biological Identity of Nanosized Materials. *Nat. Nanotechnol.* 2012, 7 (12), 779–786. https://doi.org/10.1038/nnano.2012.207.
- (28) Milani, S.; Baldelli Bombelli, F.; Pitek, A. S.; Dawson, K. A.; Rädler, J. Reversible versus Irreversible Binding of Transferrin to Polystyrene Nanoparticles: Soft and Hard Corona. ACS Nano 2012, 6 (3), 2532–2541. https://doi.org/10.1021/nn204951s.
- (29) Mahmoudi, M.; Bertrand, N.; Zope, H.; Farokhzad, O. C. Emerging Understanding of the Protein Corona at the Nano-Bio Interfaces. *Nano Today* **2016**, *11* (6), 817–832. https://doi.org/10.1016/j.nantod.2016.10.005.
- (30) Hadjidemetriou, M.; Al-Ahmady, Z.; Mazza, M.; Collins, R. F.; Dawson, K.; Kostarelos, K. In Vivo Biomolecule Corona around Blood-Circulating, Clinically Used and Antibody-Targeted Lipid Bilayer Nanoscale Vesicles. ACS Nano 2015, 9 (8), 8142–8156. https://doi.org/10.1021/acsnano.5b03300.
- (31) Wang, C.; Chen, B.; He, M.; Hu, B. Composition of Intracellular Protein Corona around Nanoparticles during Internalization. ACS Nano 2021. https://doi.org/10.1021/acsnano.0c09649.
- (32) Böhmert, L.; Voß, L.; Stock, V.; Braeuning, A.; Lampen, A.; Sieg, H. Isolation Methods for Particle Protein Corona Complexes from Protein-Rich Matrices. *Nanoscale Adv.* **2020**, 2 (2), 563–582. https://doi.org/10.1039/c9na00537d.
- (33) Zanganeh, S.; Spitler, R.; Erfanzadeh, M.; Alkilany, A. M.; Mahmoudi, M. Protein Corona: Opportunities and Challenges. *Int. J. Biochem. Cell Biol.* 2016, 75, 143–147. https://doi.org/10.1016/j.biocel.2016.01.005.
- (34) Padro, D.; Cienskowski, P.; Lopez-Fernandez, S.; Chakraborty, I.; Carrillo-Carrion, C.; Feliu, N.; Parak, W. J.; Carril, M. Toward Diffusion Measurements of Colloidal Nanoparticles in Biological Environments by Nuclear Magnetic Resonance. *Small* **2020**, *16* (36), 1–8. https://doi.org/10.1002/smll.202001160.
- (35) Cedervall, T.; Lynch, I.; Lindman, S.; Berggård, T.; Thulin, E.; Nilsson, H.; Dawson, K. A.; Linse, S. Understanding the Nanoparticle-Protein Corona Using Methods to Quntify Exchange Rates and Affinities of Proteins for Nanoparticles. *Proc. Natl. Acad. Sci. U. S. A.* **2007**, *104* (7), 2050–2055. https://doi.org/10.1073/pnas.0608582104.
- (36) Sakulkhu, U.; Maurizi, L.; Mahmoudi, M.; Motazacker, M.; Vries, M.; Gramoun, A.; Ollivier Beuzelin, M. G.; Vallée, J. P.; Rezaee, F.; Hofmann, H. Ex Situ Evaluation of the Composition of Protein Corona of Intravenously Injected Superparamagnetic Nanoparticles in Rats. *Nanoscale* 2014, 6 (19), 11439–11450. https://doi.org/10.1039/c4nr02793k.
- (37) Bertoli, F.; Davies, G. L.; Monopoli, M. P.; Moloney, M.; Gun'Ko, Y. K.; Salvati, A.; Dawson, K. A. Magnetic Nanoparticles to Recover Cellular Organelles and Study the Time Resolved Nanoparticle-Cell Interactome throughout Uptake. *Small* **2014**, *10* (16), 3307–3315. https://doi.org/10.1002/smll.201303841.
- (38) Simon, J.; Kuhn, G.; Fichter, M.; Gehring, S.; Landfester, K.; Mailänder, V. Unraveling the In Vivo Protein Corona. *Cells* **2021**, *10* (1), 1–12. https://doi.org/10.3390/cells10010132.
- (39) Blume, J. E.; Manning, W. C.; Troiano, G.; Hornburg, D.; Figa, M.; Hesterberg, L.; Platt, T. L.; Zhao, X.; Cuaresma, R. A.; Everley, P. A.; Ko, M.; Liou, H.; Mahoney, M.; Ferdosi, S.; Elgierari, E. M.; Stolarczyk, C.; Tangeysh, B.; Xia, H.; Benz, R.; Siddiqui, A.; Carr, S. A.; Ma, P.; Langer, R.; Farias, V.;

- Farokhzad, O. C. Rapid, Deep and Precise Profiling of the Plasma Proteome with Multi-Nanoparticle Protein Corona. *Nat. Commun.* **2020**, *11* (1), 1–14. https://doi.org/10.1038/s41467-020-17033-7.
- (40) Li, W.; Chen, X. Gold Nanoparticles for Photoacoustic Imaging. Nanomedicine 2015, 10 (2), 299–320. https://doi.org/10.2217/nnm.14.169.
- (41) Jin, Y.; Jia, C.; Huang, S.-W.; O'Donnell, M.; Gao, X. Multifunctional Nanoparticles as Coupled Contrast Agents. *Nat. Commun.* 2010, 1, 41.
- (42) Yue, Y.; Behra, R.; Sigg, L.; Suter, M. J. F.; Pillai, S.; Schirmer, K. Silver Nanoparticle-Protein Interactions in Intact Rainbow Trout Gill Cells. *Environ. Sci. Nano* 2016, 3 (5), 1174–1185. https://doi.org/10.1039/c6en00119j.
- (43) Melby, E. S.; Cui, Y.; Borgatta, J.; Mensch, A. C.; Hang, M. N.; Chrisler, W. B.; Dohnalkova, A.; Van Gilder, J. M.; Alvarez, C. M.; Smith, J. N.; Hamers, R. J.; Orr, G. Impact of Lithiated Cobalt Oxide and Phosphate Nanoparticles on Rainbow Trout Gill Epithelial Cells. *Nanotoxicology* 2018, 12 (10), 1166–1181. https://doi.org/10.1080/17435390.2018.1508785.
- (44) Mensch, A. C.; Mitchell, H. D.; Markillie, L. M.; Laudadio, E. D.; Hedlund Orbeck, J. K.; Dohnalkova, A.; Schwartz, M. P.; Hamers, R. J.; Orr, G. Subtoxic Dose of Lithium Cobalt Oxide Nanosheets Impacts Critical Molecular Pathways in Trout Gill Epithelial Cells. *Environ. Sci. Nano* 2020, 7 (11), 3419–3430. https://doi.org/10.1039/d0en00844c.
- (45) Wang, J.; Wu, X.; Wang, C.; Rong, Z.; Ding, H.; Li, H.; Li, S.; Shao, N.; Dong, P.; Xiao, R.; Wang, S. Facile Synthesis of Au-Coated Magnetic Nanoparticles and Their Application in Bacteria Detection via a SERS Method. ACS Appl. Mater. Interfaces 2016, 8 (31), 19958–19967. https://doi.org/10.1021/acsami.6b07528.
- (46) Tang, Y.; Liu, Y.; Li, W.; Xie, Y.; Li, Y.; Wu, J.; Wang, S.; Tian, Y.; Tian, W.; Teng, Z.; Lu, G. Synthesis of Sub-100 Nm Biocompatible Superparamagnetic Fe3O4 Colloidal Nanocrystal Clusters as Contrast Agents for Magnetic Resonance Imaging. RSC Adv. 2016, 6 (67), 62550–62555. https://doi.org/10.1039/c6ra09344b.
- (47) Duff, D. G.; Baiker, A.; Edwards, P. P. A New Hydrosol of Gold Clusters. J. Chem. Soc. Chem. Commun. 1993, No. 1, 96– 98. https://doi.org/10.1039/C39930000096.
- (48) Cox, J.; Hein, M. Y.; Luber, C. A.; Paron, I.; Nagaraj, N.; Mann, M. Accurate Proteome-Wide Label-Free Quantification by Delayed Normalization and Maximal Peptide Ratio Extraction, Termed MaxLFQ. *Mol. Cell. Proteomics* 2014, 13 (9), 2513–2526. https://doi.org/10.1074/mcp.M113.031591.
- (49) Tyanova, S.; Temu, T.; Sinitcyn, P.; Carlson, A.; Hein, M. Y.; Geiger, T.; Mann, M.; Cox, J. The Perseus Computational Platform for Comprehensive Analysis of (Prote)Omics Data. Nat. Methods 2016, 13 (9), 731–740. https://doi.org/10.1038/nmeth.3901.
- (50) Xu, M.; Soliman, M. G.; Sun, X.; Pelaz, B.; Feliu, N.; Parak, W. J.; Liu, S. How Entanglement of Different Physicochemical Properties Complicates the Prediction of in Vitro and in Vivo Interactions of Gold Nanoparticles. ACS Nano 2018, 12 (10), 10104–10113. https://doi.org/10.1021/acsnano.8b04906.
- (51) Angel, T. E.; Aryal, U. K.; Hengel, S. M.; Baker, E. S.; Kelly, R. T.; Robinson, E. W.; Smith, R. D. Mass Spectrometry-Based Proteomics: Existing Capabilities and Future Directions. *Chem. Soc. Rev.* 2012, 41 (10), 3912–3928. https://doi.org/10.1039/c2cs15331a.
- (52) Ravindra, N. M.; Tang, W.; Rassay, S. Transition Metal Dichalcogenides Properties and Applications. In Semiconductors: Synthesis, Properties and Applications; Pech-Canul, M. I., Ravindra, N. M., Eds.; Springer International Publishing: Cham, 2019; pp 333–396. https://doi.org/10.1007/978-3-030-02171-9 6.
- (53) Lundqvist, M.; Stigler, J.; Elia, G.; Lynch, I.; Cedervall, T.; Dawson, K. A. Nanoparticle Size and Surface Properties Determine the Protein Corona with Possible Implications for Biological Impacts. *Proc. Natl. Acad. Sci. U. S. A.* 2008, 105 (38), 14265–14270. https://doi.org/10.1073/pnas.0805135105.
- Zhang, H.; Burnum, K. E.; Luna, M. L.; Petritis, B. O.; Kim, J. S.; Qian, W. J.; Moore, R. J.; Heredia-Langner, A.; Webb-Robertson, B. J. M.; Thrall, B. D.; Camp, D. G.; Smith, R. D.; Pounds, J. G.; Liu, T. Quantitative Proteomics Analysis of Adsorbed Plasma Proteins Classifies Nanoparticles with

- Different Surface Properties and Size. *Proteomics* **2011**, *11* (23), 4569–4577. https://doi.org/10.1002/pmic.201100037.
- Eigenheer, R.; Castellanos, E. R.; Nakamoto, M. Y.; Gerner, K. T.; Lampe, A. M.; Wheeler, K. E. Silver Nanoparticle Protein Corona Composition Compared across Engineered Particle Properties and Environmentally Relevant Reaction Conditions. *Environ. Sci. Nano* 2014, 1 (3), 238–247. https://doi.org/10.1039/c4en00002a.
- (56) Docter, D.; Distler, U.; Storck, W.; Kuharev, J.; Wünsch, D.; Hahlbrock, A.; Knauer, S. K.; Tenzer, S.; Stauber, R. H. Quantitative Profiling of the Protein Coronas That Form around Nanoparticles. *Nat. Protoc.* 2014, 9 (9), 2030–2044.
- https://doi.org/10.1038/nprot.2014.139.
- (57) Winzen, S.; Schoettler, S.; Baier, G.; Rosenauer, C.; Mailaender, V.; Landfester, K.; Mohr, K. Complementary Analysis of the Hard and Soft Protein Corona: Sample Preparation Critically Effects Corona Composition. *Nanoscale* 2015, 7 (7), 2992–3001. https://doi.org/10.1039/c4nr05982d.
- (58) Zhang, Y.; Wu, J. L. Y.; Lazarovits, J.; Chan, W. C. W. An Analysis of the Binding Function and Structural Organization of the Protein Corona. J. Am. Chem. Soc. 2020, 142 (19), 8827– 8836. https://doi.org/10.1021/jacs.0c01853.

Insert Table of Contents artwork here

